Photoelectron Spectroscopy and Electronic Structure of ScO_n^- ($n = 1-4$) and YO_n^- ($n = 1-5$): Strong Electron Correlation Effects in ScO^- and YO^-

Hongbin Wu and Lai-Sheng Wang*,†

Department of Physics, Washington State University, 2710 University Drive, Richland, Washington 99352, and William. R. Wiley Environmental Molecular Sciences Laboratory, Pacific Northwest National Laboratory, MS K8-88, P.O. Box 999, Richland, Washington 99352

Received: June 11, 1998; In Final Form: September 9, 1998

A photoelectron spectroscopic study of ScO_n^- ($n = 1-4$) and YO_n^- ($n = 1-5$) was carried out at three photon energies: 532, 355, and 266 nm. Vibrationally resolved photoelectron spectra were obtained for ScO^- and YO^-. The electron affinities of both ScO and YO were measured to be identical (1.35 eV) within the experimental accuracy (±0.02 eV). Three low-lying excited states were observed for the monoxides, $A'^2\Delta$, $A^2\Pi$, and $B^2\Sigma^+$. The latter two excited states resulted from two-electron detachment, suggesting unusually strong electron correlation (configuration interaction) effects in the ground state of the anions. The excitation energies of the low-lying states were also found to be similar for the two monoxides except that YO has a smaller vibrational frequency and larger spin−orbit splitting. The $A'^2\Delta$ states of both ScO and YO show very strong photon energy-dependent detachment cross sections. Four similar photoelectron features were observed for the dioxides with those of YO_2^- having lower binding energies. A second isomer due to an O_2 complex was also observed for Sc and Y. Broad and featureless spectra were observed for the higher oxides. At least two isomers were present for the higher oxides, one with low and one with high binding energies.

I. Introduction

ScO is the simplest transition metal oxide with only one 3d electron. A general interest in this diatomic molecule lies in that it provides an ideal starting point for understanding the metal−oxygen bonding in the other more complicated transition metal systems. The ScO and YO diatomics have been well-studied both experimentally[1−13] and theoretically.[14−25] Their ground states are well-established, and several low-lying electronic states are known experimentally for both diatomics. However, investigation of the higher oxide molecules is rather scarce. Clemmer et al. reported an experimental measurement of the M−O bond energies and ionization potentials of MO_2 (M = Sc, Y, La) using guided ion beam reactions between MO^+ and NO_2.[26] Recently, Chertihin et al. reported an infrared study of ScO_n ($n = 1-4$) formed from reactions of laser-ablated Sc and O_2 in a low-temperature matrix.[27] Two forms of ScO_2 were observed, a bent OScO dioxide and a $Sc(O_2)$ complex. They also observed two forms of ScO_3, an $OScO_2$ molecule and a $Sc(O_3)$ ozonide species. The observed ScO_4 species was attributed to an $(O_2)Sc(O_2)$ molecule. There is no other report on the ScO_n and YO_n species.

In this paper, we present a systematic photoelectron spectroscopy (PES) study on ScO_n^- ($n = 1-4$) and YO_n^- ($n = 1-5$) to further understand the electronic structure and chemical bonding between Sc (Y) and oxygen. PES is a powerful technique to obtain size-selected electronic structure and spectroscopic information of gas-phase oxide species, providing direct measurement of the electron affinities, low-lying electronic states, and vibrational information. We have obtained vibrationally resolved PES spectra for both the mono- and dioxide species. The monoxide PES spectra of ScO^- and YO^- were found to be similar, with nearly identical binding energies. Strong two-electron detachment transitions were observed in the PES spectra of ScO^- and YO^-, suggesting unusually strong electron correlation (configuration interaction) effects in the anionic ground states. Weak detachment features due to anionic excited states were also observed in the PES spectra of the monoxides. We observed four similar detachment features for the dioxide species with those of YO_2^- having lower electron binding energies. Isomers due to O_2 complexes were also observed for the ScO_2 and YO_2 systems. We were only able to obtain very broad and featureless spectra for the higher oxide species, MO_n^- ($n \geq 3$), for which at least two isomers were observed with low and high electron binding energies, respectively. The current study is an ongoing effort of this laboratory to investigate gas-phase transition metal−oxygen molecules and clusters.[28−37]

II. Experiment

The laser vaporization cluster source−magnetic-bottle PES apparatus used in this work has been described in detail before.[38,39] In this study, the ScO_n^- and YO_n^- anions were produced by vaporizing respective metal targets with a helium carrier gas containing 0.5% O_2. ScO^- and YO^- could be produced using pure helium carrier gas owing to surface oxide layers on the targets. The negative ions from the collimated supersonic beam were extracted at 90° into a time-of-flight (TOF) mass spectrometer. The anions of interest were selected and decelerated before being detached by a laser beam from a Q-switched Nd:YAG laser (532, 355, and 266 nm). Nearly 100% of the emitted electrons were collected by the magnetic bottle and analyzed by a 3.5 m long TOF tube. The measured electron TOF spectra were calibrated using the known spectrum of Cu^-. The presented electron binding energy spectra were

† Alfred P. Sloan Research Fellow.

10.1021/jp982588q CCC: $15.00
Published on Web 10/28/1998

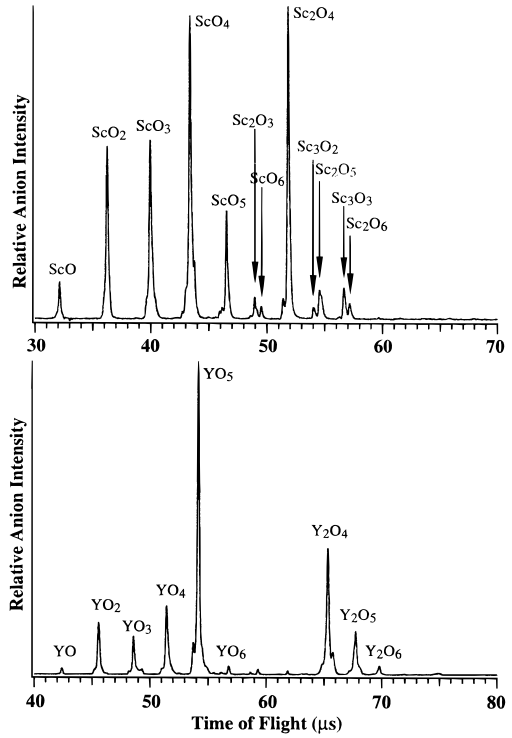

Figure 1. Time-of-flight mass spectra showing the lower mass range of $Sc_mO_n^-$ and $Y_mO_n^-$ cluster distributions when pure metal targets were laser-ablated with a 0.5% O_2/He carrier gas.

obtained by subtracting the calibrated kinetic energy spectra from the respective photon energies. Low photon energies were used to obtain better resolved spectra owing to the energy dependence of the energy resolution in the TOF-type electron analyzer. Higher photon energies were used to obtain more highly excited states of the neutral species. The resolution of the spectrometer was better than 30 meV at 1 eV electron energy.

Figure 1 shows the low mass range of typical oxide cluster mass spectra for $Sc_mO_n^-$ and $Y_mO_n^-$ when a 0.5% O_2/He carrier gas was used. In this paper, we focus on the species containing one metal atom (MO_n^-). The maximum number of oxygen atoms observed for these species was six for Sc and seven for Y under our experimental conditions. We could vary the cluster source conditions to change the relative abundance of the oxide clusters, except for ScO^- and YO^-, which were always relatively weak in all conditions. The cluster distributions also depended on the O_2 concentration. The 0.5% O_2/He carrier gas yielded maximum intensities for ScO_4^- and YO_5^- for the mono-metal oxide series (Figure 1). The abundance of ScO_6^-, YO_6^-, and YO_7^- could be slightly enhanced when the cluster source was tuned to colder conditions so that more O_2 could condense on the core, MO^- or MO_2^-. Since the highly oxygen-rich species tended to have very high electron binding energies and were not intense enough for us to obtain good quality PES spectra, only PES spectra of MO_n^- ($n \leq 4$ for Sc, $n \leq 5$ for Y) are presented and discussed.

III. Results

A. ScO^- and YO^-. Figure 2 displays the PES spectra of ScO^- at three photon energies. The 532 nm spectrum shows a well-resolved vibrational progression, representing the ground state of ScO ($X^2\Sigma^+$) and indicating that there is a bond length change between the ground states of ScO^- and ScO. Hot band (HB) transitions were also observed, yielding a vibrational

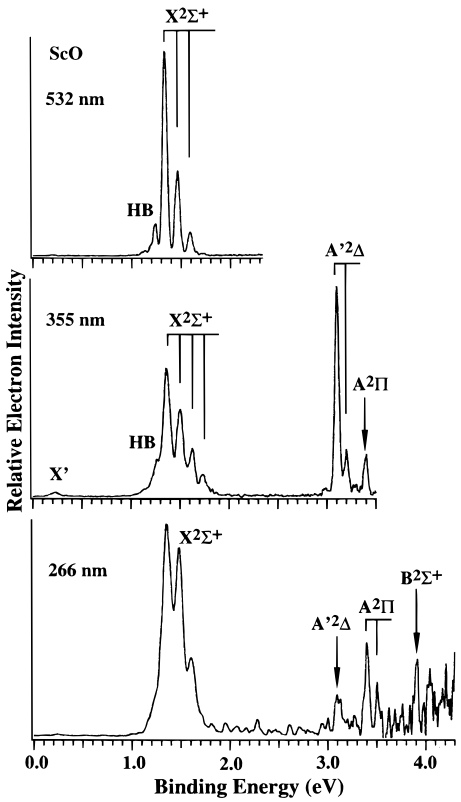

Figure 2. Photoelectron spectra of ScO^- at 532, 355, and 266 nm. HB stands for hot band transitions. Vibrational progressions are indicated with vertical lines.

frequency for the ScO^- anion to be about 840 cm^{-1}, which is considerably smaller than the vibrational frequency of the neutral ScO measured to be about 1000 cm^{-1}. This suggests that the extra electron in ScO^- enters an antibonding orbital, reducing the bond strength between Sc and O.

The 355 nm spectrum reveals an intense peak at 3.10 eV with a weak vibrational progression and an additional weak feature at ~3.4 eV. A very weak feature at low binding energy (X′) was observed in some spectra and was most likely due to an excited state of the anion. Interestingly, the sharp peak at 3.10 eV shows a strong photon energy dependence and its intensity is decreased dramatically at 266 nm, whereas the intensity of the 3.4 eV feature is enhanced slightly at 266 nm. More features at higher binding energy were also observed at 266 nm, although the signal-to-noise ratio was poor. The binding energies of all the observed states and obtained spectroscopic constants of ScO are listed in Table 1.

Figure 3 shows the PES spectra of YO^- taken at three photon energies. We observed very similar features for YO^- as for ScO^-. The 532 nm spectrum reveals a well-resolved vibrational progression for the ground state of YO. The peaks at 3.15 and 3.4 eV in the 355 nm spectrum exhibit doublet features, characteristic of a large spin−orbit splitting. A very weak low binding energy feature (X′), possibly due to an excited state of YO^-, was also present. The feature at 3.15 eV shows a strong photon energy dependence, similar to that in ScO^- (Figure 2). The 266 nm spectrum of YO^- had a low count rate and a very poor signal-to-noise ratio, and no new features can be definitively identified relative to the 355 nm spectrum. The binding energies of all the assigned states and obtained spectroscopic constants of YO are listed in Table 2.

B. ScO_2^- and YO_2^-. Figure 4 shows the spectra of ScO_2^- and YO_2^- taken at two different photon energies. The 355 nm

TABLE 1: Observed Binding Energies (BE) and Spectroscopic Constants for ScO^- and ScO

				term value (cm^{-1})		vib. freq. (cm^{-1})	
	state	configuration	BE (eV)	this work	previous[b]	this work	previous[b]
ScO^-	$X^3\Delta$	$8\sigma^2 3\pi^4 9\sigma^1 1\delta^1$	0	0		840(60)	
	$X'^1\Sigma^+$	$8\sigma^2 3\pi^4 9\sigma^2$	0.23(6)	9 000(200)			
ScO	$X^2\Sigma^+$	$8\sigma^2 3\pi^4 9\sigma^1$	1.35(2)[a]	0		1 000(50)	964.95
	$A'^2\Delta$	$8\sigma^2 3\pi^4 1\delta^1$	3.10(2)	14 200(60)	15 082.8[c]	780(70)	845.0
	$A^2\Pi$	$8\sigma^2 3\pi^4 4\pi^1$	3.40(3)	16 540(80)	16 547.0[c]	830(70)	876.0
	$B^2\Sigma^+$	$8\sigma^2 3\pi^4 10\sigma^1$	3.90(4)	20 600(100)	20 645.1		825.47

[a] Adiabatic electron affinity of ScO. [b] Reference 2. [c] Average of the two spin−orbit components.

TABLE 2: Observed Binding Energies (BE) and Spectroscopic Constants for YO^- and YO

				term value (cm^{-1})		vib. freq. (cm^{-1})	
	state	configuration	BE (eV)	this work	previous[b]	this work	previous[b]
YO	$X^3\Delta$	$11\sigma^2 5\pi^4 12\sigma^1 2\delta^1$	0	0	0	740(60)	
	$X'^1\Sigma^+$	$11\sigma^2 5\pi^4 12\sigma^2$	0.28(5)	8 600(300)			
YO	$X^2\Sigma^+$	$11\sigma^2 5\pi^4 12\sigma^1$	1.35(2)[a]	0	0	90050)	861.0
	$A'^2\Delta_{3/2}$	$11\sigma^2 5\pi^4 2\delta^1$	3.14(2)	14 500(80)	14 531.2		794.9
	$^2\Delta_{5/2}$		3.18(2)	14 800(80)	14 870.4		794.9
	$A^2\Pi_{1/2}$	$11\sigma^2 5\pi^4 6\pi^1$	3.37(4)	16 300(90)	16 315.0		820.7
	$^2\Pi_{3/2}$		3.42(4)	16 700(90)	16 742.2		822.7

[a] Adiabatic electron affinity of YO. [b] Reference 2.

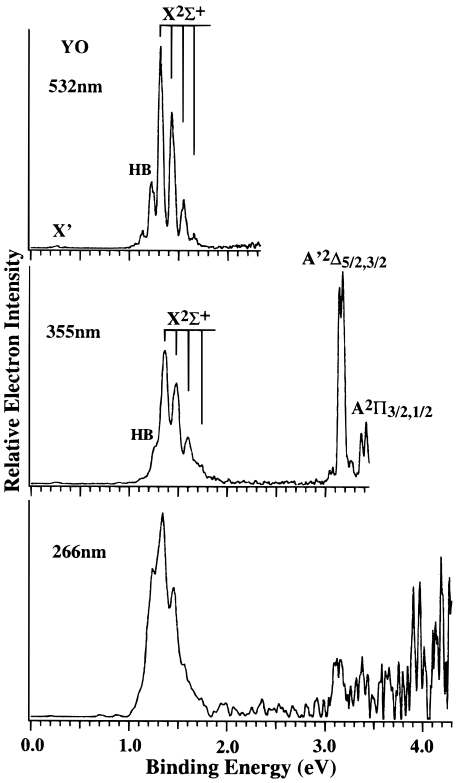

Figure 3. Photoelectron spectra of YO^- at 532, 355, and 266 nm. HB stands for hot band transitions. Vibrational progression is indicated with vertical lines.

spectrum of ScO_2^- shows two major features. The feature (X) around 2.3 eV binding energy reveals a resolved vibrational progression with a long tail in the low binding energy side. The tail may be due to either hot bands or excited states of ScO_2^- and could not be eliminated under different experimental conditions. The 266 nm spectrum of ScO_2^- reveals an additional broad feature at higher binding energies. The 355 nm spectrum of YO_2^- exhibits four resolved features with the ground-state feature (X) showing a partially resolved vibrational progression. The 266 nm spectrum of YO_2^- reveals no more new features, except for a photon energy dependence of features

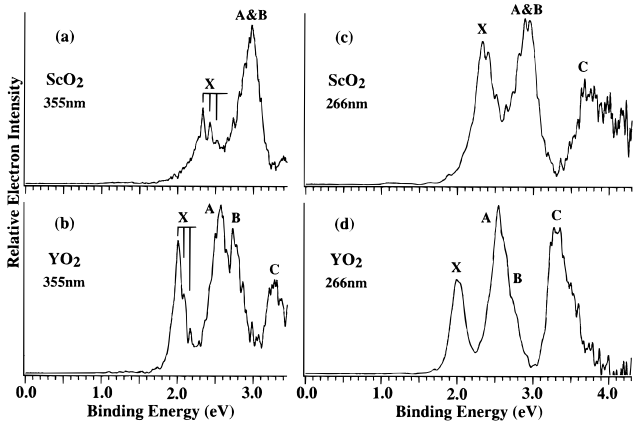

Figure 4. Photoelectron spectra of ScO_2^- and YO_2^- at 355 and 266 nm. Vibrational progressions are indicated with vertical lines.

B and C. At 266 nm, the relative intensity of feature B is decreased whereas that of feature C is enhanced. The broad low-energy tail present in the ScO_2^- spectra did not seem to be present in the YO_2^- spectra.

The 266 nm spectra of ScO_2^- and YO_2^- show remarkable similarities except that the features of the YO_2^- spectrum have lower binding energies with slightly narrower bandwidth. Comparing the two spectra, we conclude that the intense and broad feature at 2.9 eV in the ScO_2^- spectrum should contain two overlapping features (A and B), similar to the A and B features in the YO_2^- spectrum where they were resolved at 355 nm (Figure 4b). Comparing the 355 and 266 nm spectra of ScO_2^-, we can also see that the intensities of the X and A features are enhanced at 266 nm. The similarity between the dioxides of Sc and Y is analogous to that between their monoxides (Figures 2 and 3). The measured binding energies of the detachment features of ScO_2^- and YO_2^- and the obtained neutral ground-state vibrational frequencies are summarized in Table 3.

As shown in Figure 5, we sometimes could observe a weak and low-energy feature (X′) around 1.1 eV in the spectra of both ScO_2^- and YO_2^-. This weak feature was most likely due to a $M(O_2)^-$ complex, which we have observed in PES of other

TABLE 3: Observed Binding Energies (BE) and Spectroscopic Constants for ScO_2 and YO_2

	state	BE (eV)	vib. freq. (cm^{-1})[c]
ScO_2	X^2B_2, $(8a_1)^2(5b_2)^2(1a_2)^2(9a_1)^2(3b_1)^2(6b_2)^1$	2.32(2)[a]	740(80)
	A^2B_1, $(8a_1)^2(5b_2)^2(1a_2)^2(9a_1)^2(3b_1)^1(6b_2)^2$	(2.7)	
	B^2A_1, $(8a_1)^2(5b_2)^2(1a_2)^2(9a_1)^1(3b_1)^2(6b_2)^2$	(2.8)	
	C^2A_2, $(8a_1)^2(5b_2)^2(1a_2)^1(9a_1)^2(3b_1)^2(6b_2)^2$	3.6(1)	
YO_2	X^2B_2, $(13a_1)^2(6b_2)^2(2a_2)^2(14a_1)^2(5b_1)^2(7b_2)^1$	2.00(3)[b]	640(80)
	A^2B_1, $(13a_1)^2(6b_2)^2(2a_2)^2(14a_1)^2(5b_1)^1(7b_2)^2$	2.46(9)	
	B^2A_1, $(13a_1)^2(6b_2)^2(2a_2)^2(14a_1)^1(5b_1)2(7b_2)^2$	2.75(5)	
	C^2A_2, $(13a_1)^2(6b_2)^2(2a_2)^1(14a_1)^2(5b_1)^2(7b_2)^2$	3.28(6)	

[a] Adiabatic electron affinity of ScO_2. [b] Adiabatic electron affinity of YO_2. [c] ν_1 mode.

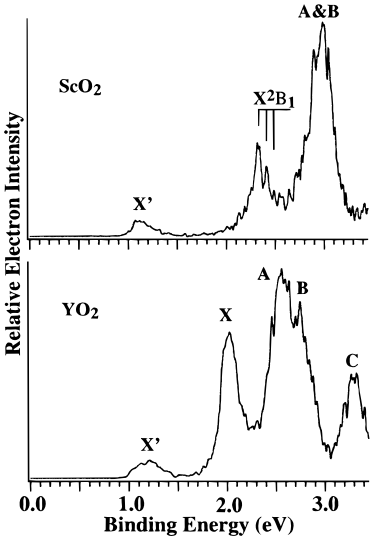

Figure 5. 355 nm photoelectron spectra of ScO_2^- and YO_2^-, showing the low binding feature (X′) due to an $M(O_2)^-$ complex.

transition metal MO_2^- systems.[29,34,35] We found that there were two conditions under which the low-energy feature could be observed. The first was when the extraction voltage for the TOF mass analysis was switched on at a late time delay. In this condition, we usually produce colder clusters because the clusters experience a slightly stronger supersonic expansion and have a longer residence time in the nozzle. The colder condition makes it easier for O_2 to condense onto the atoms, thus favoring the $M(O_2)^-$ complex formation. We could also observe the weak feature whenever we used a fresh laser-ablation target and pure helium carrier gas. In this condition, the MO_2^- species were produced from the ever-present surface oxide contamination. This latter observation may imply that oxygen prefers to adsorb on the Sc or Y surface molecularly.

C. ScO_n^- and YO_n^- ($n \geq 3$). Figure 6 shows the PES spectra of ScO_n^- ($n = 1-4$) at 355 and 266 nm, and Figure 7 shows those of YO_n^- ($n = 1-5$). We could not obtain any substantial photoelectron signals from the ScO_5^- species at either photon energy, probably owing to the high electron affinity of ScO_5 and the fact that significant noises were always present at the high binding energy side at 266 nm. The PES spectra of the higher oxide species are all quite broad without any resolvable features compared to the mono- and dioxide species. Except for that of ScO_3^-, all 355 nm spectra show low binding energy features that appear absent in the 266 nm spectra (Figures 6 and 7). Similar to those of ScO_2^- and YO_2^- as shown in Figure 5, the low binding energy features were due to minor isomers with low abundance. The dominant isomers all have much higher binding energies and could only be observed at

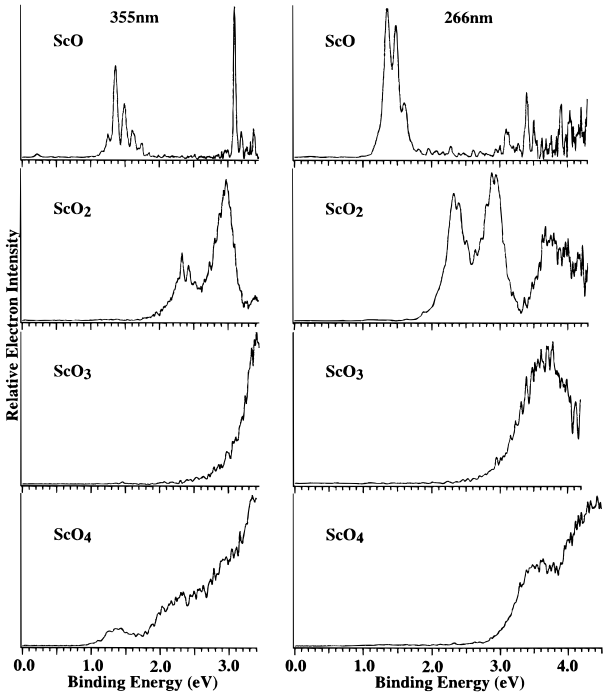

Figure 6. Photoelectron spectra of ScO_n^- ($n = 1-4$) at 355 and 266 nm.

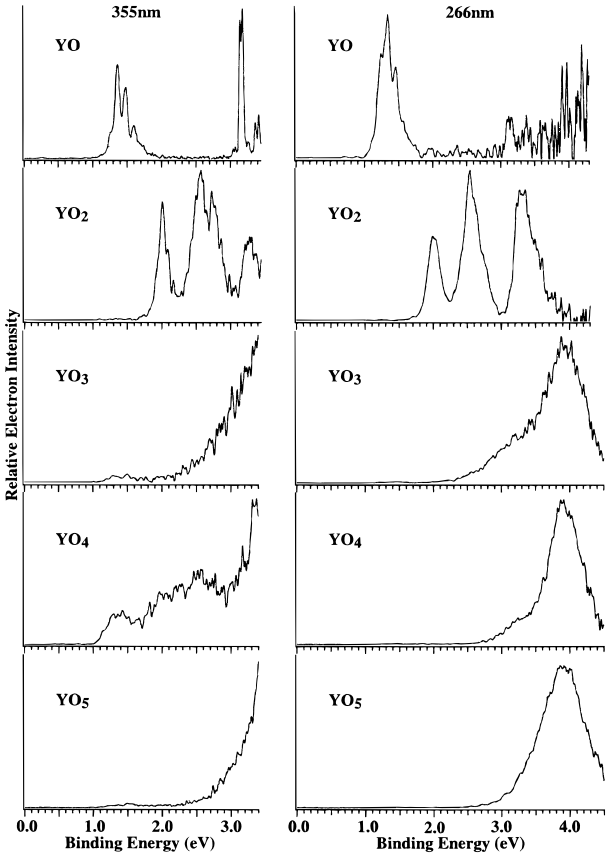

Figure 7. Photoelectron spectra of YO_n^- ($n = 1-5$) at 355 and 266 nm.

266 nm, where the low-energy features were still present but only with feeble intensities relative to the features of the main isomers. Among the low-energy features, those of ScO_4^- and YO_4^- were more prominent and they are also similar to each other with a binding energy very close to that of the $M(O_2)^-$ complexes (Figure 5).

IV. Discussion

A. ScO^- and ScO: Strong Electron Correlation Effects. The ground electronic state of ScO is well-established as $^2\Sigma^+$ with an electronic configuration of $8\sigma^2 3\pi^4 9\sigma^1$, where 8σ is from Sc 3dσ and O 2pσ, 3π is from Sc 3dπ and O 2pπ, and 9σ is mainly a nonbonding 4s orbital. The low-lying excited states of ScO are well-established, including the $A'^2\Delta$ ($8\sigma^2 3\pi^4 1\delta^1$), $A^2\Pi$ ($8\sigma^2 3\pi^4 4\pi^1$), and $B^2\Sigma^+$ ($8\sigma^2 3\pi^4 10\sigma^1$).[1-4] All of these states were observed in the PES spectra of ScO^-, as shown in Figure 2. The obtained term values and vibrational frequencies are in good agreement with known values from the literature,[1-4] as shown in Table 1.

The extra electron in the ground state of ScO^- can enter either 9σ to give a singlet anion ground state or a 1δ orbital to give a triplet state. Since ScO^- is isoelectronic to TiO, which possesses a $^3\Delta$ (...$9\sigma^1 1\delta^1$) ground state,[1] it is reasonable to assume that the extra electron in ScO^- enters the 1δ orbital. Thus the following detachment channels would be necessary to reach the neutral excited states observed in the PES spectra:

$$8\sigma^2 3\pi^4 9\sigma^1 1\delta^1\ (^3\Delta) \rightarrow 8\sigma^2 3\pi^4 9\sigma^1 \quad X^2\Sigma^+ \quad (1)$$

$$\rightarrow 8\sigma^2 3\pi^4 1\delta^1 \quad A'^2\Delta \quad (2)$$

$$\rightarrow 8\sigma^2 3\pi^4 4\pi^1 \quad A^2\Pi \quad (3)$$

$$\rightarrow 8\sigma^2 3\pi^4 10\sigma^1 \quad B^2\Sigma^+ \quad (4)$$

The detachment channels 1 and 2 result from one-electron transition from the 1δ and 9σ orbitals, respectively. The observed photon energy dependence of the $X^2\Sigma^+$ and $A'^2\Delta$ PES features are consistent with these detachment channels in that the detachment cross section for removing electrons with high angular momenta increase with photon energies.[40] The spin-orbit splitting[2] of the $A'^2\Delta$ state is known to be 106.1 cm^{-1}, which is too small to be resolved under our experimental resolution.

However, both detachment channels 3 and 4 require two-electron transitions. Such multielectron transitions, due to strong electron correlation effects, have been observed in PES of TiO^-.[36] It is unusual to see that the intensities of the $A^2\Pi$ and $B^2\Sigma^+$ features have even stronger intensities than that of the $A'^2\Delta$ feature in the 266 nm spectrum (Figure 2). This observation suggests strong electron correlation effects in the ScO^- ground state ($^3\Delta$), which must have strong configuration mixings. PES has been the primary experimental technique to investigate electron correlation effects by observing such multielectron transitions, usually called photoelectron "satellite".[41] However, ScO^- is the first example with such clear and strong "satellite" features in an anionic molecular system. We have previously reported a strong two-electron transition in the PES of Cu^- at 193 nm.[34]

Our obtained term values and vibrational frequencies are in excellent agreement with those from the literature, except for that of the term value for the $A'^2\Delta$ state. Our measured value is smaller than the literature value by exactly a vibrational quantum. The literature value was derived from emission spectra of the $A'^2\Delta$ to the ground state in a chemiluminescence experiment.[1-4] We suspect that the origin band was misassigned in the previous work.

The weak feature labeled as X′ is assigned to a transition from an electronic excited state of ScO^- to the ground state of neutral ScO. We tentatively assign this anion excited state to be $8\sigma^2 3\pi^4 9\sigma^2$ ($^1\Sigma^+$), where the extra electron enters the 9σ orbital to give a singlet state. This excited state is expected to be metastable as it is spin-forbidden for it to relax down to the anion ground state. We have observed such metastable anionic excited states in several transition metal diatomic systems previously.[34,36,37]

B. YO^- and YO. The PES spectra of YO^- are almost identical to that of ScO^- except for a slight larger spin-orbit splitting in the $^2\Delta$ and $^2\Pi$ states, which were well within our resolution (Figure 3). It is surprising that the electron affinity of YO is identical to that of ScO within our experimental accuracy, and even the term values of the low-lying states of YO are rather close to those of ScO, as given in Table 2. Thus the PES spectra of YO^- can be assigned similarly, as shown in Figure 3. Analogous to ScO^-, the ground state of YO^- should be $X^3\Delta$ with a $11\sigma^2 5\pi^4 12\sigma^1 2\delta^1$ configuration. Single-electron detachment of the 2δ and 12σ electron results in the $X^2\Sigma^+$ and $A'^2\Delta$ states, respectively. The $A^2\Pi$ state would require a two-electron transition from the anion ground state, similar to the detachment channel 3 in ScO^-. The 266 nm spectrum of YO^- had very low count rate and poor signal-to-noise ratio, which prevent us from making definitive assignments of any higher excited states. However, the feature near 3.9 eV yields a term value, which is very close to the literature value (20 791 cm^{-1}) for the $B^2\Sigma^+$ state. Our obtained term values and vibrational frequencies are listed in Table 2 and are in excellent agreement with those from the literature.

C. MO_2 (M = Sc and Y). There has been no theoretical work concerning the electronic structure of either ScO_2 or YO_2. In the recent low-temperature matrix infrared study,[27] Chertihin et al. used density functional theory to calculate the structure and vibrational frequencies of ScO_2. They found that ScO_2 is a bent molecule with a bond angle of 128° and a $^2B_2$ ground state. Their calculated ν_1 vibrational frequency is 742 cm^{-1}, which is in good agreement with our measured ν_1 frequency of 740(80) cm^{-1}. To understand and interpret the PES spectra and electronic structure of ScO_2, we can use the previous results of TiO_2 and VO_2, which we have recently studied.[36,37] Both are similar to ScO_2 with a bent structure except that they have one and two extra 3d electrons compared to ScO_2. Particularly, there has been a very recent study on the electronic structure of VO_2 using ab initio calculations.[42]

The chemical bonding between Sc and O is mainly from the interactions between the Sc 3d and 4s and the O 2p. Using the result of VO_2 by subtracting two valence electrons,[42] we get the following valence configuration for ScO_2: $(8a_1)^2(5b_2)^2(1a_2)^2$-$(9a_1)^2(3b_1)^2(6b_2)^1$ with a $^2B_2$ ground state, consistent with the result of Chertihin et al., who obtained a $^2B_2$ ground state for ScO_2. In ScO_2^-, the extra electron most likely enters the $6b_2$ orbital to give a closed-shell ground state for the anion. Therefore, the PES features of ScO_2^- are interpreted in the single-particle picture to be due to detachment of an electron from the top four valence molecular orbitals, respectively, as shown in Table 3. The PES spectra of YO_2^- are similarly interpreted (Table 3), except that the valence molecular orbitals of YO_2 are formed from the Y 4d and 5s and O 2p. The PES spectra of ScO_2^- and YO_2^- are relatively simple because of the closed-shell nature of the anion ground states. The low-energy tail present in the spectra of ScO_2^- is probably due to excited states of ScO_2^- because they could not be eliminated by better vibrational cooling. Similar low-energy tails were also observed in the PES spectra of VO_2^- previously.[37] It is interesting to note that the binding energies of all the YO_2^- PES features are lower than those of ScO_2^- whereas the PES features of the monoxides (Figures 2 and 3) are almost identical. We suspect that the destabilization of the YO_2 valence molecular

orbitals relative to those of ScO_2 may be due to the fact that they have different bond angles. The 4d and 5s orbitals of Y are more spatially diffuse compared to the 3d and 4s orbital of Sc and may lead to a larger bond angle for YO_2.

Figure 5 shows evidence for an MO_2 isomer, which we assigned to an $M(O_2)$ complex. This isomer possesses a much lower electron affinity, comparable to those of the monoxides. The $Sc(O_2)$ complex was observed in the previous matrix study.[27] Transition metal−dioxygen complexes have been observed in our previous PES studies of transition metal oxides, such as $Cu(O_2)$[29,34] and $Ni(O_2)$.[35] We have found that the $M(O_2)$ complexes always have lower electron affinities than the OMO dioxides and similar electron affinities to the respective monoxides. The O_2 in the $Sc(O_2)$ and $Y(O_2)$ complexes is likely side-bonded to the metal atom and can be viewed as a peroxide (O_2^{2-}), somewhat analogous to the monoxide in term of the formal oxidation state of the metal, explaining their similar electron affinities.

D. MO_n ($n \geq 3$) (M = Sc and Y). The PES spectra of the higher oxide molecules are compared to the mono- and dioxides in Figures 6 and 7 for ScO_n^- ($n = 1-4$) and YO_n^- ($n = 1-5$), respectively. The spectra of the higher oxide species are quite broad and featureless and only a few qualitative remarks can be made. It is seen that the electron binding energies increase from MO^- to MO_3^-. The binding energies of MO_3^- are so high that only a tail was observed in the 355 nm spectra. The 266 nm spectrum of ScO_3^- shows a broad feature and long low-energy tail whereas that of YO_3^- appears to have a lower (~3 eV) and a higher (~4 eV) binding energy feature, both very broad. In the previous matrix study of Sc/O_2, two ScO_3 species were identified, an ozonide $Sc(O_3)$ and an $(O_2)ScO$ species.[27] In the latter, the O_2 is side-bonded to Sc to give a C_{2v} molecule. We assign the observed PES spectra of MO_3^- to the C_{2v} isomer. In the 355 nm spectrum of YO_3^-, very weak signals were discernible between 1 and 1.5 eV binding energies, which was probably due to the ozonide isomer of YO_3. However, we did not seem to observe a similar ozonide isomer of ScO_3^- with any substantial abundance. The ScO_3 and YO_3 species are similar to CuO_3, for which we have observed both the ozonide and C_{2v} isomers previously.[34]

The 355 nm spectra of both ScO_4^- and YO_4^- are similar, both with broad low-energy features, which seem to disappear in the 266 nm spectra, where only high binding energy features were observed. The low-energy features are in fact still present in the 266 nm spectra with much weaker relative intensities, suggesting that the lower binding energy features were due to a minor isomer. An $(O_2)Sc(O_2)$ complex was identified in the previous matrix study.[27] The electron affinity of the minor isomer is quite low, similar to that of the $M(O_2)$ complexes (Figure 5). Therefore, it is reasonable to assign the minor isomer of MO_4 to be an $(O_2)M(O_2)$ species, where O_2 is head-bonded to the metal (superoxide-like). We tentatively assign the major MO_4^- isomer to one in which the O_2 molecules are side-bonded to the metal atom (peroxide-like). Hence the formal oxidation state of the metal is higher in the major isomer, consistent with its high electron affinity.

The 355 nm spectrum of YO_5^- appeared similar to that of YO_3^-, with some very weak signals between 1 and 2 eV binding energies and a high-energy tail. The 266 nm of YO_5^- shows a broad peak, which seems to be similar to that in both YO_3^- and YO_4^- (Figure 7). Again the very weak low energy signals present in the 355 nm spectrum were probably due to a minor isomer. The YO_5^- mass signal could be made very strong in our source, as shown in Figure 1. We tentatively assign the major isomer to be $(O_2)_2YO$. The broad nature of the PES spectra of all the higher oxides suggests that these species are probably rather floppy with significant geometry changes between the anions and the neutrals.

V. Conclusions

We report a systematic photoelectron spectroscopic study of the isoelectronic ScO_n ($n = 1-4$) and YO_n ($n = 1-5$) oxide species. Electron affinities and excitation energies of low-lying electronic excited states were measured for the mono- and dioxide species. We found that ScO and YO have identical electron affinities within our experimental accuracy and very similar excitation energies for their excited states. Vibrationally resolved spectra were obtained for the monoxides and an anionic excited state was also observed. Unusually strong two-electron detachment transitions were observed for ScO^- and YO^-, suggesting strong correlation effects and configuration mixings in the ground states of ScO^- and YO^-. The PES spectra of ScO_2^- and YO_2^- were also similar, with that of YO_2^- having lower binding energies. Isomers due to $M(O_2)^-$ complexes were observed for both Sc and Y systems, which have much lower electron binding energies close to the monoxides. Very broad and featureless spectra were obtained for the higher oxide species, which were due to different O_2 complexes of the metal atom and monoxide.

Acknowledgment. Support for this research from the National Science Foundation is gratefully acknowledged. The work is performed at Pacific Northwest National Laboratory, operated for the U.S. Department of Energy by Battelle under Contract DE-AC06-76RLO 1830.

References and Notes

(1) Merer, A. J. *Annu. Rev. Phys. Chem.* **1989**, *40*, 407.
(2) Huber, K. P.; Herzberg, G., *Molecular Spectra and Molecular Structure IV: Constants of Diatomic Molecules*; Van Nostrand Reinhold: New York, 1979.
(3) Chalek, C. L.; Gole, J. L. *J. Chem. Phys.* **1976**, *65*, 2845.
(4) Chalek, C. L.; Gole, J. L. *Chem. Phys.* **1977**, *19*, 59.
(5) Rice, S. F.; Field, R. W. *J. Mol. Spectrosc.* **1986**, *119*, 331.
(6) Rice, S. F.; Childs, W. J.; Field, R. W. *J. Mol. Spectrosc.* **1989**, *133*, 22.
(7) Hoeft, J.; Torring, T. *Chem. Phys. Lett.* **1993**, *215*, 367.
(8) Simard, B.; James, A. M.; Hacket, P. A. *J. Mol. Spectrosc.* **1992**, *154*, 455.
(9) Steimle, T. C.; Shirley, J. E. *J. Chem. Phys.* **1990**, *92*, 3298.
(10) Suenram, R. D.; Lovas, F. J.; Fraser, G. T.; Matsumura, K. *J. Chem. Phys.* **1990**, *92*, 4724.
(11) Childs, W. J.; Poulsen, O.; Steimle, T. C. *J. Chem. Phys.* **1988**, *88*, 598.
(12) Steimle, T. C.; Alramadin, Y. *J. Mol. Spectrosc.* **1987**, *122*, 103.
(13) Linton, C. *J. Mol. Spectrosc.* **1978**, *69*, 351.
(14) Bakalbassis, E. G.; Stiakaki, M. D.; Tsipis, A. C.; Tsipis, C. A. *Chem. Phys.* **1996**, *205*, 389. Jeung, G. H.; Koutecky, J. *J. Chem. Phys.* **1988**, *88*, 3747.
(15) Bauschlicher, Jr., C. W.; Langhoff, S. R. *J. Chem. Phys.* **1986**, *85*, 5936.
(16) Dolg, M.; Wedig, U.; Stoll, H.; Preuss, H. *J. Chem. Phys.* **1987**, *86*, 2123.
(17) Mattar, S. M., *J. Phys. Chem.* **1993**, *97*, 3171; Piechota, J.; Suffczynski, M. *Z. Phys. Chem.* **1997**, *200*, 39.
(18) Andzelm, J.; Radzio, E.; Barandiaran, Z.; Seijo, L. *J. Chem. Phys.* **1985**, *83*, 4565.
(19) Bauschlicher, C. W., Jr.; Maitre, P. *Theor. Chim. Acta* **1995**, *90*, 189.
(20) Pettersson, L.; Wahlgren, U. *Chem. Phys.* **1982**, *69*, 185.
(21) Pettersson, L.; Wahlgren, U.; Gropen, O. *Chem. Phys.* **1983**, *80*, 7.
(22) Green, D. W. *J. Phys. Chem.* **1971**, *75*, 3103.
(23) Pettersson, L.; Stromberg, A. *Chem. Phys. Lett.* **1983**, *99*, 122.
(24) Huzinaga, S.; Klobukowski, M.; Sakai, Y. *J. Phys. Chem.* **1984**, *88*, 4880.

(25) Langhoff, S. R.; Bauschlicher, C. W., Jr. *J. Chem. Phys.* **1988**, *89*, 2160.
(26) Clemmer, D. E.; Dalleska, N. F.; Armentrout, P. B. *Chem. Phys. Lett.* **1992**, *190*, 259.
(27) Chertihin, G. V.; Andrews, L.; Rosi, M.; Bauschlicher, C. W., Jr. *J. Phys. Chem.* **1997**, *101*, 9085.
(28) Fan, J.; Wang, L. S. *J. Chem. Phys.* **1995**, *102*, 8714.
(29) Wu. H.; Desai, S. R.; Wang, L. S. *J. Chem. Phys.* **1995**, *103*, 4363.
(30) Wang, L. S., Fan, J.; Lou, L. *Surf. Rev. Lett.* **1996**, *3*, 695.
(31) Wang, L. S., Wu, H.; Desai, S. R.; Lou, L. *Phys. Rev. B* **1996**, *53*, 8028.
(32) Wu., H.; Desai, S. R.; Wang, L. S. *J. Am. Chem. Soc.* **1996**, *118*, 5296.
(33) Wang, L. S.; Wu, H.; Desai, S. R. *Phys. Rev. Lett.* **1996**, *76*, 4853.
(34) Wu, H.; Desai, S. R.; Wang, L. S. *J. Phys. Chem. A* **1997**, *101*, 2103.
(35) Wu, H.; Wang, L. S. *J. Chem. Phys.* **1997**, *107*, 16.
(36) Wu, H.; Wang, L. S. *J. Chem. Phys.* **1997**, *107*, 8221.
(37) Wu, H.; Wang, L. S. *J. Chem. Phys.* **1998**, *108*, 5310.
(38) Wang, L. S., Cheng, H.; Fan, J. *J. Chem. Phys.* **1995**, *102*, 9480.
(39) Wang, L. S.; Wu, H. In *Advances in Metal and Semiconductor Clusters*; Duncan, M. A., Ed.; JAI Press: Greewich, CT, 1998; Vol. 4, p 299.
(40) Hufner, S. *Photoelectron Spectroscopy*; Springer-Verlag: New York, 1995; p 15.
(41) Suzer, S.; Lee, S. T.; Shirley, D. A. *Phys. Rev.* A **1976**, *13*, 1842.
(42) Knight, L. B., Jr.; Babb, R.; Ray, M.; Banisaukas, T. J., III; Russon, L.; Dailey, R. S.; Davidson, E. R. *J. Chem. Phys.* **1996**, *105*, 10, 237.